

## Combining Time-Resolved Hard X-ray Diffraction and Diffuse Reflectance Infrared Spectroscopy To Illuminate CO Dissociation and Transient Carbon Storage by Supported Pd Nanoparticles during CO/NO Cycling

Mark A. Newton,<sup>\*,†</sup> Marco Di Michiel,<sup>†</sup> Anna Kubacka,<sup>‡</sup> and Marcos Fernández-García<sup>\*,‡</sup>

ESRF, 6 Rue Horowitz, BP-220, Grenoble F-38043, France, and Instituto de Catálisis y Petroleoquímica, CSIC, C/Marie-Curie 2, 28049 Madrid, Spain

Received December 21, 2009; E-mail: newton@esrf.fr; mfg@icp.csic.es

A novel combination of time-resolved hard X-ray diffraction (HXRDX) with diffuse reflectance infrared spectroscopy (DRIFTS) and mass spectrometry (MS) that takes advantage of the intrinsic properties of very high energy X-rays has been developed for use in studying gas-solid interactions. The method has allowed us to specify how Al<sub>2</sub>O<sub>3</sub>-supported Pd nanoparticles (~3 nm diameter) actively participate in prototypical de-NO<sub>x</sub> chemistry. We show that unresolved issues in the behavior of this system observed using time-resolved extended X-ray absorption fine structure (EXAFS)<sup>1</sup> during CO/NO cycling are due to the dissociation of adsorbed CO species and transient storage of atomic carbon within the Pd nanoparticles, forming PdC<sub>x</sub>. This bulk PdC<sub>x</sub> phase is then rapidly removed during the oxidizing (NO) part of the cycle. Furthermore, it is shown that the formation of PdC<sub>x</sub> promotes the formation of linear CO species on the surface of the changing nanoparticles and has a drastic effect on the linear-to-bridge ratio observed in the IR spectra.

Many functional materials, including heterogeneous catalysts, show structural variation on a wide range of length scales, from chemical bonds through nanosized component phases to the micrometer scale. This provides a strong driving force for devising experiments capable of addressing these varied length scales and provide “holistic” structure–function relationships.<sup>2</sup> As such, the sequential combination of X-ray methods (principally diffraction/scattering and EXAFS) has a long history.<sup>3–6</sup> These previous methods have generally relied upon X-ray energies below 20 keV and/or a restricted number of sample environment types (quartz capillaries and tubes)<sup>4–7</sup> to obtain the angular range necessary for diffraction measurements. Even recent studies that have started to exploit high-energy X-rays for diffraction<sup>7,8</sup> and total scattering analyses<sup>9</sup> of working catalysts have retained this methodology. Here we take a different approach that permits synchronous investigation of the sample using DRIFTS in order to achieve the same net objective within a highly restrictive sample environment.

At very high X-ray energies, because of the Bragg diffraction condition ( $\lambda/d = 2 \sin \theta$ ), a compression of diffraction peaks into smaller solid angles occurs. As a result, at ~86.8 keV ( $\lambda = 0.143 \text{ \AA}$ ) we can collect a large  $Q$  ( $\text{\AA}^{-1}$ ) range [see the Supporting Information (SI)] using an experimental setup subtending only ca.  $\pm 10^\circ$  previously developed<sup>10</sup> for combining transmission EXAFS (a technique that has no solid-angle requirements for data collection) with DRIFTS and MS. Our previous investigations allowed us to start to understand the dynamic structure–reactivity behavior of small supported Pd nanoparticles.<sup>1</sup> However, a number of observations remained to be precisely quantified (e.g., size/shape/disorder change) or even explained. In the latter category, the source of a

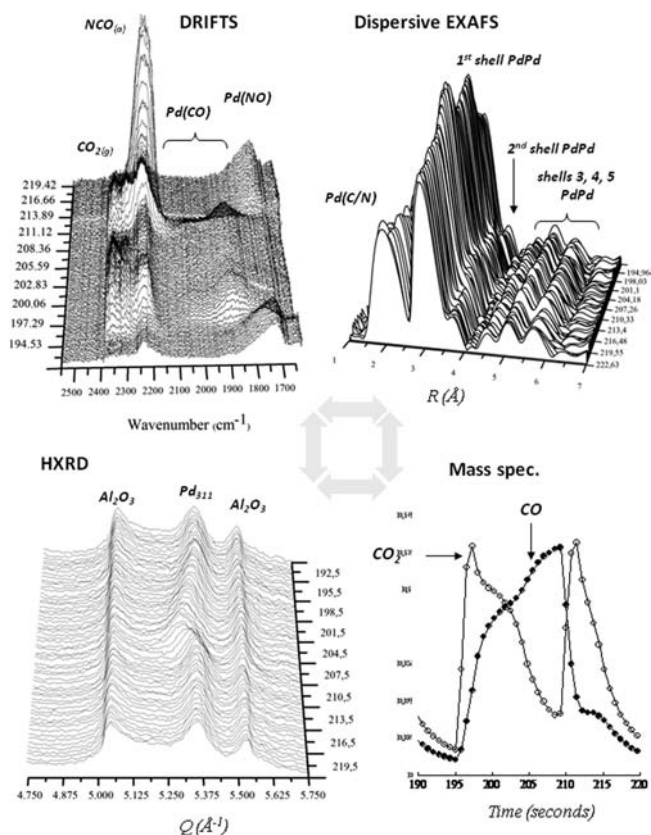


**Figure 1.** Illustrative data from the four probes DRIFTS, EXAFS, MS, and HXRDX (the [311] reflection from Pd, straddled by two Al<sub>2</sub>O<sub>3</sub> reflections) that can be applied in situ using the current methodology. Each of the X-ray techniques may be used in simultaneous time-resolved conjunction with DRIFTS and MS. The data from each technique pertain to the structure–reactivity behavior of a 2 wt % Pd/Al<sub>2</sub>O<sub>3</sub> sample during a single switch from 5% CO/He to 5% NO/He at 673 K (see the SI).

pronounced fall and then recovery of the first-shell Pd–Pd EXAFS coordination number was left unresolved from structural and reactive points of view.<sup>1</sup> An example of this behavior (as observed using dispersive EXAFS) is shown in Figure 1 (top right, first-shell Pd–Pd central depression) for a 2 wt % Pd/Al<sub>2</sub>O<sub>3</sub> sample during CO/NO cycling at 673 K.

Alongside the dispersive EXAFS data, Figure 1 shows a salient portion (see the SI) of the HXRDX data that can now be obtained simultaneously with the DRIFTS and MS measurements in the same apparatus. The data for a single CO/NO cycle were extracted from an overall experiment of the type previously described<sup>1</sup> (see the SI).

<sup>†</sup> ESRF.

<sup>‡</sup> Instituto de Catálisis y Petroleoquímica.

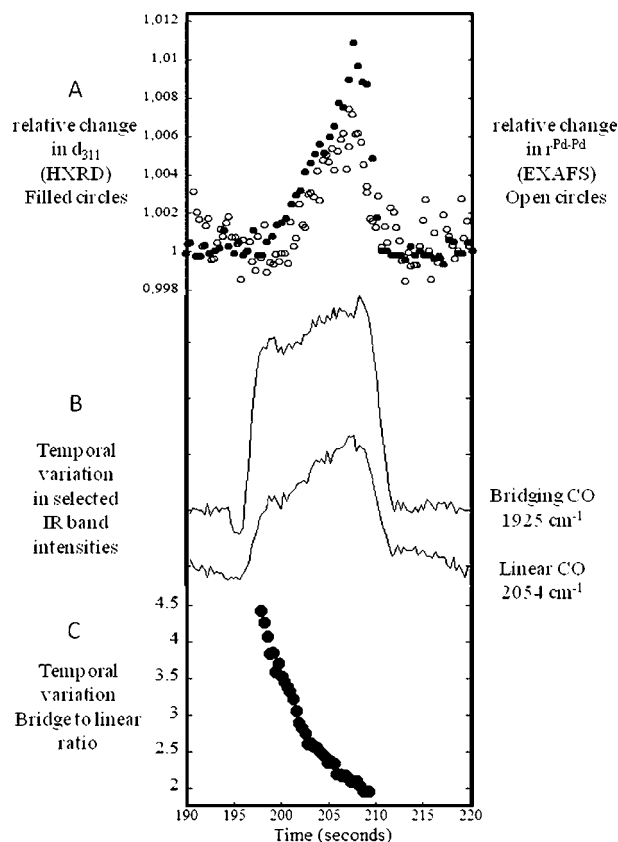


**Figure 2.** Temporal behavior of 2 wt % Pd/Al<sub>2</sub>O<sub>3</sub> during the NO/CO/NO cycle at 673 K. (A) Relative change in the first-shell Pd–Pd distance (EXAFS) and  $d$  spacing of the Pd[311] reflection (HXRD). (B) Intensity of bridging and linear CO bands (DRIFTS). (C) Bridging CO to linear CO ratio (DRIFTS) during the CO cycle.

The HXRD data reveal an increase (essentially linear in time during the CO cycle) in the  $d$  spacing of the visible XRD reflections ([111], [200], [311], [222]) due to the Pd nanoparticles (see the SI). Such a process is not immediately evident from the EXAFS or the DRIFTS data. Only the MS data initially hint at this via a secondary phase of CO<sub>2</sub> production after the gas switch. Upon the switch back to NO, the  $d$  spacing returns to the initial point of the cycle.

Figure 2 shows other elements that can be extracted from the combined experiments as a function of time. A more formal analysis of the EXAFS data from Figure 1, along with a more precise measurement of the temporal character and magnitude of the observed changes in the  $d$  spacing ([311] reflection) in the HXRD pattern, quantifies an expansion of the Pd lattice from both local and long-range order points of view (Figure 2A). This isotropic lattice expansion (see the SI) is indicative of a bulk change in the Pd phase and quantitatively consistent with the dissolution of atomic carbon into the nanoparticles to form a PdC<sub>*x*</sub> phase with  $0.05 \leq x \leq 0.06$ .<sup>11</sup>

This resolves the apparent behavior of the Pd–Pd coordination number observed during the CO cycle<sup>1</sup> shown in Figure 1. The changes in the static disorder of the system associated with the formation<sup>12</sup> and destruction of PdC<sub>*x*</sub> would result in these apparent coordination number changes within the paradigms of the EXAFS analysis.<sup>1</sup> However, without a priori knowledge of such chemistry, it is only the application of the HXRD that allows us to specify that this is the case. In X-ray absorption near-edge structure (XANES), the formation of PdC<sub>*x*</sub><sup>12</sup> results in no change in the Pd K-edge position and only small changes in the position of the 1s → 5p ( $\Delta E = 1.2$  eV) and 1s → 4f ( $\Delta E = 0.3$  eV) resonances (see the SI).<sup>12</sup>

Furthermore, the combination of XRD, DRIFTS, and MS establishes that during the CO cycle, where IR spectroscopy tells us that the Pd nanoparticles are covered in linear and bridging CO, some of these CO molecules dissociate. The atomic C thus formed migrates into the bulk of the Pd nanoparticles (HXRD). The atomic oxygen formed from the CO dissociation reacts with adsorbed CO to create the second stage of CO<sub>2</sub> evolution (MS, Figure 1). At the same time DRIFTS (Figure 2) shows that the growth of the linear CO species is highly correlated with the formation of the expanded PdC<sub>*x*</sub> phase, whereas this is not the case for the bridging CO. As a result, as carbon dissolves into the Pd lattice, the linear-to-bridging ratio changes significantly (Figure 2C). This results from the promotion of the occupation of linear CO sites, possibly as a result of a morphological change in the nanoparticles accompanying the formation of the PdC<sub>*x*</sub> phase. As the bridging-to-linear ratio in IR spectra is commonly used to estimate the Pd particle size (e.g., see ref 13), our combined results show that this notion could be severely misleading under actual reaction conditions.

In summary, using a new experiment that combines time-resolved HXRD (or transmission EXAFS) with DRIFTS and MS for the in situ study of gas–solid interactions, we have demonstrated how such a combination can yield significantly enhanced insight into fundamental events occurring in nanoparticulate catalysts. We have elucidated rapid CO dissociation over Pd nanoparticles and the subsequent storage of atomic C in the bulk of these particles that results from this event. Under NO, the PdC<sub>*x*</sub> phase is readily removed as CO<sub>2</sub>, closing the catalytic cycle. We have also dynamically followed how the in situ formation of the PdC<sub>*x*</sub> phase changes the populations of CO species that are adsorbed on the Pd, with the formation of linear CO being significantly promoted by the change in Pd phase.

**Acknowledgment.** We thank ESRF for access to facilities (ID24, ID15B). A.K. thanks CSIC for an I3P (JAE Doc) postdoctoral grant.

**Supporting Information Available:** Experimental setup, energy resolution of the dispersive EXAFS experiment at the Pd K edge, sampling by EXAFS/XRD, and factors influencing comparability. This material is available free of charge via the Internet at <http://pubs.acs.org>.

## References

- (1) Newton, M. A.; Belver-Coldeira, C.; Martínez-Arias, A.; Fernández-García, M. *Nat. Mater.* **2007**, *6*, 528.
- (2) Weckhuysen, B. M. *Angew. Chem., Int. Ed.* **2009**, *48*, 4910.
- (3) Couves, J. W.; Thomas, J. M.; Waller, D.; Jones, R. H.; Derbyshire, G. E.; Greaves, G. N. *Nature* **1991**, *354*, 465.
- (4) Clausen, B. S.; Grabaek, L.; Steffensen, G.; Hansen, P. L.; Topsøe, H. *Catal. Lett.* **1993**, *20*, 20.
- (5) Clausen, B. S.; Topsøe, H.; Frahm, R. *Adv. Catal.* **1998**, *42*, 315.
- (6) Beale, A. M.; van der Eerden, A. M. J.; Jacques, S. D. M.; Leynaud, O.; O'Brien, M. G.; Meneau, F.; Nikitenko, S.; Bras, W.; Weckhuysen, B. M. *J. Am. Chem. Soc.* **2006**, *128*, 12386.
- (7) Beale, A. M.; Jacques, S. D. M.; Berfwerff, J. A.; Barnes, P.; Weckhuysen, B. M. *Angew. Chem., Int. Ed.* **2007**, *46*, 8832.
- (8) O'Brien, M. G.; Beale, A. M.; Jacques, S. D. M.; Di Michiel, M.; Weckhuysen, B. M. *ChemCatChem* **2009**, *1*, 99.
- (9) Chupas, P. J.; Chapman, K. W.; Jennings, G.; Lee, P. L.; Grey, C. P. *J. Am. Chem. Soc.* **2007**, *129*, 13822.
- (10) Newton, M. A. *Top. Catal.* **2009**, *52*, 1410.
- (11) (a) Ziemecki, S. B.; Jones, G. A.; Swartzfager, G. D.; Harlow, R. A.; Faber, J., Jr. *J. Am. Chem. Soc.* **1985**, *107*, 4547. (b) Maciejewski, M.; Baiker, A. *J. Phys. Chem.* **1994**, *98*, 285.
- (12) McCaulley, J. A. *J. Phys. Chem.* **1993**, *97*, 10372.
- (13) For instance, see: (a) Martínez-Arias, A.; Hungria, A. B.; Fernández-García, M.; Iglesias Juez, A.; Anderson, J. A.; Conesa, J. C. *J. Catal.* **2004**, *221*, 85. (b) Schalow, T.; Brandt, B.; Starr, D. E.; Laurin, M.; Shaikhudinov, S. K.; Schauermaann, S.; Libuda, J.; Freund, H.-J. *Phys. Chem. Chem. Phys.* **2007**, *9*, 1347.

JA9107512